THE JOURNAL OF PHYSICAL CHEMISTRY C

ARTICLE

pubs.acs.org/JPCC

On the Formation and the Structure of the First Bimetallic Borohydride Borate, $LiCa_3(BH_4)(BO_3)_2$

Young-Su Lee,*[,†] Yaroslav Filinchuk,[‡,§] Hyun-Sook Lee,[†] Jin-Yoo Suh,[†] Ji Woo Kim,[†] Jong-Sung Yu,[∥] and Young Whan Cho[†]

[†]Future Convergence Research Division, Korea Institute of Science and Technology, Seoul 136-791, Republic of Korea

[‡]Institute of Condensed Matter and Nanosciences, Université Catholique de Louvain, Place L. Pasteur, B-1348, Louvain-la-Neuve, Belgium

[§]Swiss-Norwegian Beamlines at ESRF, BP-220, 38043 Grenoble, France

[∥]Department of Advanced Materials Chemistry, WCU Research Center, Korea University, 208 Seochang, Jochiwon, Chungnam 339-700, Republic of Korea

ABSTRACT: We present the first report on the formation and the crystal structure of a bimetallic borohydride borate, $LiCa_3(BH_4)(BO_3)_2$. It is discovered during decomposition of $LiBH_4-Ca(BH_4)_2$–carbon composite studied for hydrogen storage. A small amount of oxygen impurity in the starting material or introduced during sample preparation gives rise to the formation of $[BO_3]^{3-}$. Its crystal structure was solved from synchrotron powder diffraction data as space group $Fd\bar{3}m$ and a = 14.5911(2) Å at 387 °C. The experimental structural parameters are closely reproduced and the orientational disorder in $[BH_4]^-$ is confirmed by first-principles calculations.

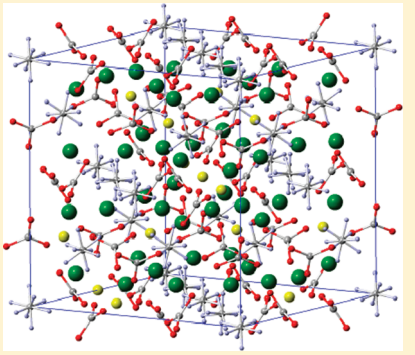

1. INTRODUCTION

Metal borohydrides, $M(BH_4)_n$, have been intensively studied for reversible hydrogen storage due to their high volumetric and gravimetric hydrogen density.[1−3] On top of their technical importance, the crystal structures of metal borohydrides are especially intriguing since the versatility of $[BH_4]^-$ groups in coordinating metal cations brings a variety of crystal structures, many of which have only recently been discovered and solved.[4−13]

While those new structures have drawn theoretical and experimental interests, complex structures occasionally with unknown chemical compositions often delay identifying the reaction sequences during dehydrogenation or rehydrogenation. One example is $Ca(BH_4)_2$; the final product was identified to be CaB_6 and CaH_2, but the intermediate steps still remain to be clarified.[14−20]

Recently, hydrogen storage properties of $LiBH_4-Ca(BH_4)_2$, which forms a eutectic melt, was investigated.[21,22] The major dehydrogenation event was observed at lower temperature compared to the constituting borohydrides, but the detailed reaction mechanism was not satisfactorily explained, one of the reasons being an unidentified compound found at around 240−400 °C. That compound is a single solid phase at that temperature range since the major phase $LiBH_4-Ca(BH_4)_2$ is in liquid. It was speculated to be partially decomposed $Ca(BH_4)_2$, CaB_mH_n, due to the similarity in X-ray diffraction (XRD) peak positions at low angles and in thermal behavior to those of an unidentified phase appearing during decomposition of $Ca(BH_4)_2$.[21,23] In this study, with high resolution XRD patterns we solved the crystal structure and determined the composition of the unidentified compound. To our surprise, it turned out to be $LiCa_3(BH_4)(BO_3)_2$; the presence of $[BO_3]^{3-}$ is unexpected since no explicit oxygen source exists in starting materials. From the view of hydrogen storage in $LiBH_4-Ca(BH_4)_2$, the formation of this compound is undesirable. However, the crystal structure itself is very interesting, and to the best of our knowledge it is the first example of a bimetallic borohydride borate. We discuss the crystal structure solution in detail; a first-principles study complements the experimental diffraction study.

2. EXPERIMENTAL SECTION

2.1. Synthesis. The starting materials are $LiBH_4$ (assay 95%, Acros), $Ca(BH_4)_2$ (assay 98%, Sigma-Aldrich), and mesoporous carbon. Mesoporous carbon (CMK-3) was synthesized by replication through nanocasting of ordered mesoporous silica template.[24,25] The average pore size was 3.6 nm. The materials were handled in an argon-filled glovebox (LABstar, MBraun, $p(O_2, H_2O) < 1$ ppm) if necessary. A mixture of $0.75LiBH_4 + 0.25Ca(BH_4)_2$ (in molar ratio)

Received: February 7, 2011
Revised: April 8, 2011
Published: April 28, 2011

dx.doi.org/10.1021/jp2012232 | J. Phys. Chem. C 2011, 115, 10298–10304

Table 1. Experimental and DFT Calculated Structural Parameters of $LiCa_3(BH_4)(BO_3)_2$

	structure	atom	Wyckoff symbol	x	y	z	U_{iso} (Å^2)	occupation
experimental	$Fd\bar{3}m$	Li	16*d*	0.5000	0.5000	0.5000	0.190(16)	1.0
	a = 14.5911(2) Å	Ca	48*f*	0.38968(11)	0.1250	0.1250	0.0553(6)	1.0
		B1	32*e*	0.2760(5)	0.2760(5)	0.2760(5)	0.007(4)	1.0
		O	96*g*	0.23963(12)	0.23963(12)	0.34956(14)	0.0523(8)	1.0
		B2	16*c*	0.0000	0.0000	0.0000	0.089(8)	1.0
		H1	32*e*	−0.0455	−0.0455	−0.0455	0.089(8)	0.5
		H2	96*g*	−0.0152	−0.0152	0.0758	0.089(8)	0.5
calculated	$Fd\bar{3}m$	Li	16*d*	0.5000	0.5000	0.5000		1.0
	a = 14.59 Å	Ca	48*f*	0.3937	0.1250	0.1250		1.0
		B1	32*e*	0.2755	0.2755	0.2755		1.0
		O	96*g*	0.2379	0.2379	0.3541		1.0
		B2	16*c*	0.0000	0.0000	0.0000		1.0
		H1	32*e*	−0.0484	−0.0484	−0.0484		0.5
		H2	96*g*	−0.0135	−0.0135	0.0819		0.5

and the same weight of mesoporous carbon were mixed together. The carbon content was chosen such that the mesopore volume (1.15 cm^3/g) is similar to the volume of the metal borohydride mixture. About 1 g of the mixture was ball-milled with three 12.7 mm and seven 7.9 mm diameter Cr-steel balls. The ball-milling was conducted using a planetary mill (Fritsch P7) at 600 rpm for 1 h.

2.2. In Situ Synchrotron X-ray Diffraction (XRD). In situ synchrotron XRD measurements were carried out at the 10B· XRS KIST-PAL beamline in Pohang Accelerator Laboratory. The selected X-ray wavelength was 1.00001 Å. A sapphire tube (o.d. = 1.52 mm, i.d. = 1.07 mm) was used as a sample holder. The sample was first heat-treated to induce infiltration of mixed borohydrides into the mesoporous carbon. Temperature was raised from room temperature (RT) to 190 °C in 20 min and then slowly increased up to 215 °C in 30 min, and then was held for 10 min. The sample was cooled down to RT. For dehydrogenation, temperature was raised at a rate of 2 °C/min from RT up to 540 °C. The hydrogen pressure was maintained at 3 bar. XRD patterns were collected every 147 s during the in situ experiement with a MAR345 image plate detector. The two-dimensional (2D) images were converted into 1D diffraction data by the FIT2D program.[26]

2.3. Structure Solution. Diffraction peaks were indexed in face-centered cubic cell and the data were fitted by le Bail method with a = 14.5911(2) Å. Systematic absences suggested space groups $Fd\bar{3}m$ and $Fd\bar{3}$, which were tested in the course of a structure solution by global optimization in direct space (program FOX[27]). The structure was solved by optimizing position of one Ca atom, one Li atom, one BH_4 group, and a position and orientation of one BO_3 group, all in special positions. Soft antibump restraints Li...H > 2.2 Å, Ca...H > 2.4 Å, and H...H > 2.2 Å were applied. While the presence of other atomic species are expected from the chemical composition of the starting materials, the BO_3 groups were included for the following reason: the optimized geometries systematically showed a presence of flat triangular B_4 units and the refinement of atomic occupancies suggested that the atoms in the corners are heavier than the one in the center, which can be most reasonbly interpreted if B_4 units are BO_3 groups.

The final refinement was made by Rietveld method, using program Fullprof.[28] Only four free coordinate parameters were refined, along with group B-factors for Li, Ca, B, O, and B(H) (see Table 1). The BH_4 group is disordered over two orientations in the high-symmetry $\bar{3}m$ position, and it can not be ordered in the lower symmetry $Fd\bar{3}$ space group. Positions of the two independent hydrogen atoms are fully determined by the point group symmetry of the tetrahedral BH_4 group combined with the crystallographic site symmetry, and the B−H distances are fixed at 1.15 Å.[29] Therefore, coordinates of H-atoms were not refined, but later validated by density functional theory (DFT) methods. The BO_3 group has a nearly perfect flat geometry (unrestrained) with B−O distances close to the expected value. The agreement factors are R_B = 7.8%, R_{wp} (not corrected for background) = 0.78%, R_{wp} (corrected for background) = 6.15%, and χ^2 = 456. The high value of χ^2 reflects mainly the extremely high counting statistics (signal-to-noise ratio) of the powder diffraction data obtained from the 2D detector.

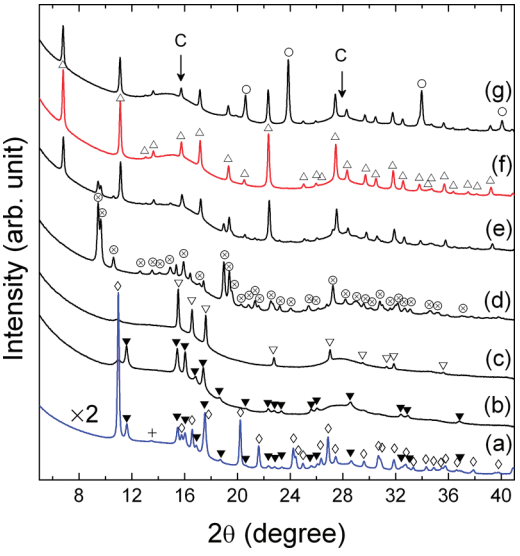

Figure 1. Synchrotron XRD diffraction pattern at (a) RT as-milled (shown in 50% of the original intensity), (b) RT after infiltration, (c) 126 °C, (d) 240 °C, (e) 270 °C, (f) 387 °C, and (g) 427 °C. The symbols for each phase are (▼) o-$LiBH_4$, (▽) h-$LiBH_4$, (◊) α-$Ca(BH_4)_2$, (+) γ-$Ca(BH_4)_2$, (⊗) $Ca_3(BH_4)_3(BO_3)$, (Δ) $LiCa_3(BH_4)(BO_3)_2$, (○) CaO.

Table 2. Experimental and DFT Calculated Selected Interatomic Distances and Angles[a]

	experimental	calculated	number	other compounds
Li−O	2.206(2)	2.143	6	[b]1.940−2.032, [d]2.004−2.225
Ca−O	2.437(2)^{I}	2.400^{I}	2	[c]2.347−2.440, [d]2.361−2.512
	2.483(2)^{II}	2.446^{II}	4	
B1−O	1.310(8)	1.385	3	[b]1.369−1.383, [c]1.384
Ca−B1	2.851(7)	2.813	2	[c]2.808, [d]2.886
Ca−B2	3.287(1)	3.324	2	[e]2.816−2.967
Ca−H2	2.450(1)^{I}	2.471^{I}	2	[e]2.227−2.806
	2.828(1)^{II}	2.844^{II}	4	
B2−H1	1.15	1.223	1	[e]1.158−1.181
B2−H2		1.227	3	
Li−O−B1	139.5(3)	139.23		[b]84.35−167.08
Ca−O−B1	138.9(3)^{I}	138.01^{I}		[c]90.15−135.23
	92.2(3)^{II}	90.11^{II}		
O−B1−O	120.00	119.96		[b]119.21−120.38, [c]119.95
Ca−H2−B2	128.14^{I}	124.52^{I}		[e]86.27−116.59
	103.21^{II}	102.04^{II}		
H1−B2−H2	109.47	112.14		[e]107.60−113.06
H2−B2−H2		106.67		

[a] The units are Å for the distances and degree for the angles. The superscripts in Roman numbers are to differentiate between crystallographically independent interatomic distances and angles. The number of equivalent bonds is shown in the fourth column. [b] Li_3BO_3[46] [c] $Ca_3(BO_3)_2$[47] [d] $LiCaBO_3$[45] [e] α-$Ca(BH_4)_2$[10]

2.4. First-Principles Calculation. The experimental structure solution was reoptimized by first-principles calculations. The calculations were done within the framework of density functional theory (DFT),[30,31] as implemented in the Vienna Ab-initio simulation package.[32,33] The generalized-gradient approximation by Perdew, Burke, and Ernzerhof[34] was adopted for exchange-correlation functional. Projector augmented wave potential[35] with a planewave cutoff energy of 600 eV was used. Atomic coordinates were optimized until the force on each atom becomes smaller than 0.005 eV/Å. The *k*-point meshes were chosen such that the total energy converges within 0.1 meV/atom.

3. RESULTS AND DISCUSSION

3.1. Chemistry and Crystal Structure. Figure 1 presents the XRD patterns before and after heat treatment and during dehydrogenation of the $LiBH_4-Ca(BH_4)_2$−carbon sample. The mesoporous carbon is introduced to improve hydrogen storage properties of the $LiBH_4-Ca(BH_4)_2$ composite via nanoconfinement,[36,37] but we herein limit ourselves to the chemisty and the crystal structure of the title compound, leaving the hydrogen storage properties as a separate work. The initial mixture (Figure 1a) mainly consists of α-$Ca(BH_4)_2$ and *o*-$LiBH_4$. The two broad humps marked by the arrows are from the mesoporous carbon.[38,39] After heat treatment at 215 °C (Figure 1b), the peaks of α-$Ca(BH_4)_2$ disappeared except for the broad main peak, which serves as an indirect evidence that $Ca(BH_4)_2$ was infiltrated into the mesoporous carbon[36,37] when the $LiBH_4-Ca(BH_4)_2$ eutectic melt was formed. The remaining $LiBH_4$ indicates that the present composition is off the eutectic point and is located in the $LiBH_4$-rich side. Upon raising the temperature, *o*-$LiBH_4$ was transformed into *h*-$LiBH_4$ (Figure 1c) and then the phase called δ-$Ca(BH_4)_2$[17,40] was formed (Figure 1d). Recently δ-$Ca(BH_4)_2$ was identified to be $Ca_3(BH_4)_3(BO_3)$,

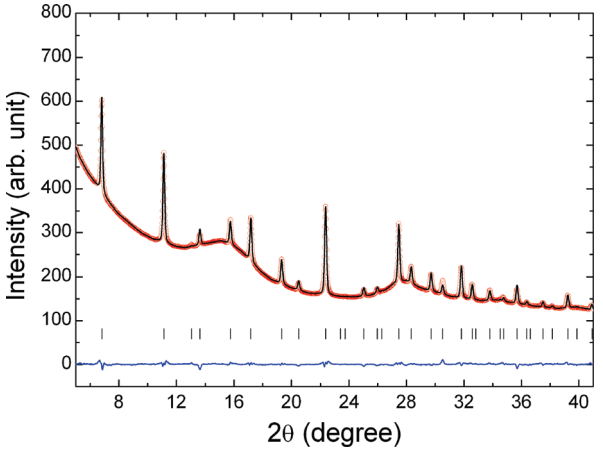

Figure 2. Synchrotron XRD diffraction pattern in Figure 1f (red dots) and the fit (black line) obtained by Rietveld method.

which is another case of metal borohydride borate.[41] At around 250 °C, the title compound started to grow while consuming $Ca_3(BH_4)_3(BO_3)$ (Figure 1e). The title compound was the single solid phase in the temperature range of 300−400 °C (Figure 1f) before CaO was formed (Figure 1g). We emphasize that the major components, $LiBH_4$ and $Ca(BH_4)_2$, were not detected by XRD since they were in the liquid state. One can notice that the XRD peak intensity of the title compound is much smaller than that of the starting material.

As aforementioned, the structure solution assigns a chemical formula of $LiCa_3(BH_4)(BO_3)_2$ to the title compound. The final structural parameters from Rietveld method are summarized in Table 1 and the selected interatomic distances and angles in Table 2. The Rietveld plot is shown in Figure 2. The presence of $[BO_3]^{3-}$ is somewhat unexpected since there is no explicit

Table 3. Experimental and DFT Calculated Molar Volume of Several Metal Borohydrides and Borates[a]

V/Z (Å^3)	experimental	calculated
o-$LiBH_4$	54.17[51]	53.12
α-$Ca(BH_4)_2$	105.91 (−182 °C)[10]	107.2
α-Li_3BO_3	62.31[46]	63.12
$Ca_3(BO_3)_2$	127.60[47]	130.4
$LiCa_3(BH_4)(BO_3)_2$	194.15 (387 °C)	194.0

[a] The experimental temperature is RT if not noted.

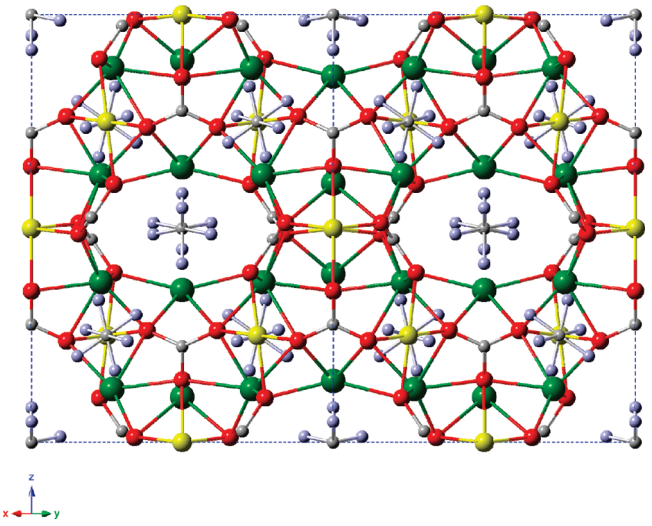

Figure 3. Crystal structure of $LiCa_3(BH_4)(BO_3)_2$ viewed along [110] direction. Li, Ca, B, O, and H atoms are colored in yellow, olive, gray, red, and light blue, respectively.

source of oxygen. Oxygen impurity contained in the starting materials or introduced during sample handling must be responsible for the formation of $[BO_3]^{3-}$. The mesoporous carbon may provide a certain amount of oxygen impurity but is not a single source of oxygen since the title compound was previously observed in the $LiBH_4-Ca(BH_4)_2$ mixture without carbon.[21] In addition, the intermediate phase II reported in the study of 1:1 $LiBH_4-Ca(BH_4)_2$ mixture by Fang et al.[42] is likely to be $LiCa_3(BH_4)(BO_3)_2$ judging from the XRD peak positions. It is not uncommon to observe oxygen containing species such as CaO in the course of dehydrogenation of $Ca(BH_4)_2$.[40,43] As briefly mentioned above, the very recent identification of "δ-$Ca(BH_4)_2$" being a borohydride borate, $Ca_3(BH_4)_3(BO_3)$, highlights the importance of this type of partially dehydrogenated and oxidized form of metal borohydrides. The sequential formation of $Ca_3(BH_4)_3(BO_3)$ and $LiCa_3(BH_4)(BO_3)_2$ hints at a variety of metal borohydride borates different in cation combination or $[BH_4]^-$ to $[BO_3]^{3-}$ ratio.

We now turn our attention to the stability of $LiCa_3(BH_4)(BO_3)_2$. There exist at least two Li−Ca bimetallic borates, $Li_4Ca(BO_3)_2$ and $LiCa(BO_3)$,[44,45] together with the constituting monometallic borates, Li_3BO_3[46] and $Ca_3(BO_3)_2$.[47] In the case of borohydrides, a recent work proposed the existence of $LiCa(BH_4)_3$, but its structure has not been identified yet.[42] The formation reactions of $LiCa_3(BH_4)(BO_3)_2$ from the known monometallic borohydrides and

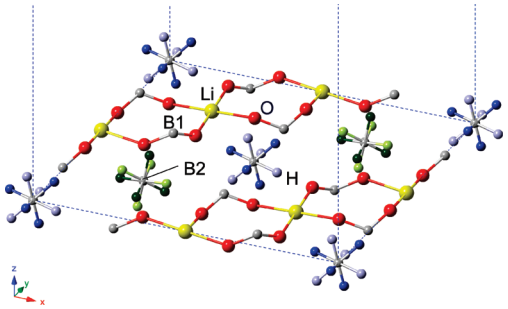

Figure 4. A cross section of the structure in (001) plane. The two different orientations are indicated either in dark or in light blue (green).

borates can be written as follows

$$o\text{-}LiBH_4 + Ca_3(BO_3)_2 \rightarrow LiCa_3(BH_4)(BO_3)_2, \quad \Delta E = -0.09 \text{ eV} \tag{1}$$

$$2\ \alpha\text{-}Li_3BO_3 + 3\ \alpha\text{-}Ca(BH_4)_2 \rightarrow LiCa_3(BH_4)(BO_3)_2 + 5\ o\text{-}LiBH_4, \quad \Delta E = -0.91 \text{ eV} \tag{2}$$

The calculated negative reaction energies only tell us that once $[BO_3]^{3-}$ anions are formed they prefer to constitute the complex title compound rather than to reside in the simple monometallic borates. The above reactions, however, do not reflect the actual mechanism in our experiment since we found neither Li_3BO_3 nor $Ca_3(BO_3)_2$ that preceded $LiCa_3(BH_4)(BO_3)_2$. From the XRD patterns in Figure 1, a more plausible reaction sequence is the following

$$LiBH_4\ (l) + 2\ Ca_3(BH_4)_3(BO_3)\ (s) \rightarrow LiCa_3(BH_4)(BO_3)_2\ (s) + 3\ Ca(BH_4)_2\ (l) \tag{3}$$

In fact, the formation of the borohydride borates accompanies a small amount of hydrogen release and weight loss,[21] and thus $[BO_3]^{3-}$ anions may not be introduced as metal borates from the starting materials and would mainly be a product of on-site oxidation of $[BH_4]^-$. While it is not of interest in this work, this partially oxidized borohydride borate may find its use in chemical or electrochemical oxidation process of borohydride.[48]

In terms of the coordination environment, $LiCa_3(BH_4)(BO_3)_2$ resembles more Li_3BO_3 and $Ca(BH_4)_2$ than $Ca_3(BO_3)_2$ and $LiBH_4$ since Li is exclusively surrounded by six O atoms (donated by six different $[BO_3]^{3-}$ groups) and so is $[BH_4]^-$ by six Ca atoms. The coordination numbers, however, are not identical to those in the monometallic salts; in Li_3BO_3 each Li is coordinated by four, not six, O atoms and the Li...O distance is 1.94−2.03 Å, which is shorter than 2.206 Å in $LiCa_3(BH_4)(BO_3)_2$. The Ca...B2 distance of 3.287 Å in $LiCa_3(BH_4)(BO_3)_2$ is much longer than 2.82−2.97 Å in α-$Ca(BH_4)_2$ in which $[BH_4]^-$ is coordinated by three Ca atoms (see Table 2).[10] The slightly expanded first coordination shell and the increased number of coordinating atoms mean that the coordinated atom takes up a larger volume. Indeed, the calculated molar volume of the product side is larger by 10.5 Å^3 in reaction (1) and by 11.8 Å^3 in reaction (2) (see Table 3). The open channel along [110] direction in Figure 3 reflects a rather loose packing in $LiCa_3(BH_4)(BO_3)_2$ especially around the $[BH_4]^-$ groups, and therefore the compound may exhibit a rather fast $[BH_4]^-$ diffusion.

3.2. Structure Optimization by First-Principles Calculation and $[BH_4]^-$ Orientation. First-principles calculations were

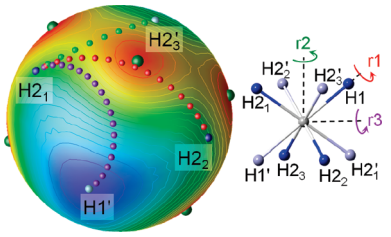

Figure 5. Electrostatic potential projected on a sphere of r = 1.226 Å centered at the origin. The color changes from blue to red as the electrostatic potential decreases. Hydrogen atoms are drawn in the same color scheme as in Figure 4. Small spheres show the trajectory of rotation around **r1** (red), **r2** (green), and **r3** (violet) axes. Olive spheres are projected Ca atoms.

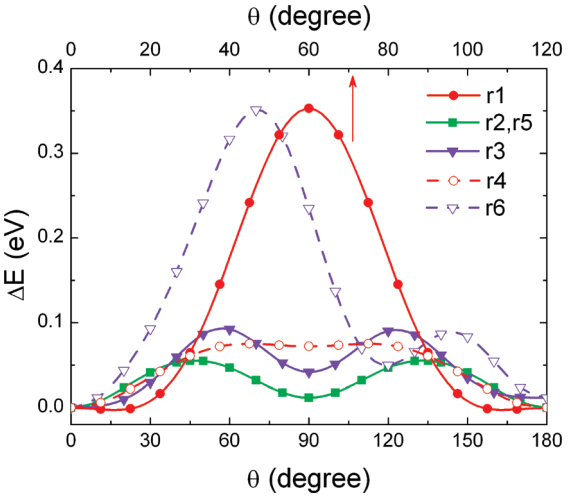

Figure 6. Energy change upon rotation of $[BH_4]^-$ around the six rotational axes. The top axis is for the two 3-fold axes (**r1** and **r4**).

carried out to confirm the structural stability of $LiCa_3(BH_4)(BO_3)_2$. In setting up the simulation cell, a complication entered due to the proposed two $[BH_4]^-$ orientations with half occupancy (see Table 1). The most realistic way of describing the disorder would be a molecular dynamics simulation so that the atomic coordinates can be extracted from the time average. Instead, we took a simplified approach, where static calculations were carried out on a few combinations of $[BH_4]^-$ orientations. The orientations of the sixteen $[BH_4]^-$ groups in the cubic unit cell are uniquely determined by two inequivalent $[BH_4]^-$ groups if face-centered and rhombohedral symmetries are imposed. The two inequivalent $[BH_4]^-$ groups are colored in blue and green in Figure 4, and the two orientations are shown in dark and light tones. Four combinations are possible: dark blue/light green (**c1**), dark blue/dark green (**c2**), light blue/light green (**c3**), and light blue/dark green (**c4**). Among those, **c1** is symmetrically equivalent to **c4**, and so is **c2** to **c3**. Assigning the orientation in this way reduces the symmetry from $Fd\bar{3}m$ to $R3m$ space group. The atomic coordinates were optimized under the constraints of $\alpha = \beta = \gamma = 90°$ and fixed Li and B2 positions in order not to introduce too many degrees of freedom. The lattice parameter at the total energy minimum was calculated to be 14.59 Å for both **c1** (**c4**) and **c2** (**c3**), which is in close agreement with the experimental value. The DFT-calculated atomic coordinates summarized in Table 1 were obtained from the average of the four combinations. The individual coordinates again closely reproduce the experimental values.

It may seem that too many constraints were forced to simplify the disorder, which could introduce artifacts to the calculation results, but it turned out that total energy and the structural parameters are not so sensitive to the $[BH_4]^-$ orientation. The energy difference between **c1** and **c2** is as small as 5 meV/f.u. (0.3 meV/atom), and even after removing all the above constraints the volume varies within 0.1% with the rhombohedral angle virtually remaining at 90°. The small difference in energy between **c1** and **c2** indicates a tendency toward disorder since there is no strong correlation in the orientation of the nearby $[BH_4]^-$ groups. The shortest B2...B2 distance is as large as 5.158 Å, and therefore the orientation would rather be determined by other ionic species positioned more closely. Since the bonding is largely ionic, a simple electrostatic potential map may provide a good insight on H positions and energy barrier for the reorientation. We choose the cubic unit cell of the **c1** configuration and remove one $[BH_4]^-$ group at the origin. The uncompensated positive charge is neutralized by a uniform background charge. Figure 5 shows the electrostatic potential at r = 1.226 Å, which is the calculated average B−H bonding distance from the origin. The point symmetry at the origin is $3m$ without inversion symmetry, but it largely preserves $\bar{3}m$ character though the absolute values would not exactly conform to that symmetry, again confirming the weak dependence on the six nearest $[BH_4]^-$ groups. The color on the surface gradually changes from blue to red as the electrostatic potential decreases; the blue color corresponds to the lowest energy since H in $[BH_4]^-$ is negatively charged.[49,50] Isopotential lines are drawn with an interval of 0.08 V. We can easily locate two H1 positions at the two energy minima in blue, which are the crossing points on the sphere by the [111] vector. Then the H2 atoms locate themselves in the green-colored region such that they are most distant from the energy maxima in red while keeping the overall tetrahedral geometry of $[BH_4]^-$. The fundamental potential distribution is mostly governed by the closest 6 Ca^{2+} ions: they fall almost exactly on the maxima when projected onto the sphere as drawn in olive spheres in Figure 5. The H2 atoms prefer to be surrounded by 3 Ca^{2+} rather than to point directly to a single Ca^{2+}. Even the slight deviation of the calculated ∠H1−B2−H2 = 112.1° from the ideal angle (109.5°) can be understood from the potential map since the larger angle allows H2 to lower its energy.

Now we place the $[BH_4]^-$ group back at the origin and calculate the energy variation upon the rotation. The result is summarized in Figure 6. Six axes of rotation are defined as follows: **r1** = $\overrightarrow{H1}$, **r2** = $\overrightarrow{H1} + \overrightarrow{H2_1}$, **r3** = $\overrightarrow{H1} - \overrightarrow{H2_1}$, **r4** = $\overrightarrow{H2_1}$, **r5** = $\overrightarrow{H2_1} + \overrightarrow{H2_2}$, and **r6** = $\overrightarrow{H2_1} - \overrightarrow{H2_2}$. The indices of H atoms and the trajectories of the rotations are shown in Figure 5. The geometry of $[BH_4]^-$ is fixed to be an ideal tetrahedron with B−H distance of 1.226 Å, and the atomic coordinates of all other atoms are frozen. The energy variation upon the rotation again can be guessed from the electrostatic potential. For instance, in the case of **r1**, all three H2 atoms are bound to pass the high energy region in red (see Figure 5), which is reflected in the large energy barrier of 0.35 eV. The rotation around the two 3-fold axes, **r1** and **r4**, does not reorient the $[BH_4]^-$ group. Rotation by 90° around **r2** or **r5**, or 180° around **r3** or **r6**, converts the dark-toned H positions into the light-toned H′ ones or vice versa. The lowest energy barrier for the reorientation found in **r2** or **r5** is 0.055 eV, a magnitude that can be easily overcome by thermal energy in the temperature range where $LiCa_3(BH_4)(BO_3)_2$ is observed. The **r3**

rotation offers a higher barrier of 0.092 eV and the **r6** rotation is as unfavorable as **r1**. In fact, the real energy barrier would become even smaller when the atoms are allowed to move, supporting the random orientation of $[BH_4]^-$ from the structure solution.

4. CONCLUSIONS

A new compound $LiCa_3(BH_4)(BO_3)_2$ was found and its crystal structure was determined using synchrotron powder diffraction data and DFT calculations. Structural parameters obtained from first-principles calculation closely reproduce the experimental values. The formation of this complex compound is favorable with respect to the constituting monometallic borohydrides and borates. The random orientation of $[BH_4]^-$ is examined by first-principles calculation. The upper bound of the barrier for the reorientation is as small as 0.055 eV, confirming the structure solution which suggests disordered $[BH_4]^-$ groups. The present structure solution corrects the previous misinterpretation of the unidentified compound found during decomposition of $LiBH_4-Ca(BH_4)_2$ and leads us toward a better understanding of the $LiBH_4-Ca(BH_4)_2$ mixture studied for hydrogen storage. Consideration of this type of compound could also be relevant in identifying some of the still unknown compounds reported in other metal borohydrides.

AUTHOR INFORMATION

Corresponding Author
*E-mail: lee0su@kist.re.kr.

ACKNOWLEDGMENT

This work has been sponsored by the Hydrogen Energy R&D Center, one of 21st Century Frontier R&D Programs funded by the Ministry of Education, Science and Technology of Korea and NRF Grant (MEST: 2009-0077413). The authors gratefully acknowledge the support by Ik Jae Lee and Keun Hwa Chae at the KIST-PAL beamline for the in situ synchrotron XRD measurements.

REFERENCES

(1) Züttel, A.; Wenger, P.; Rentsch, S.; Sudan, P.; Mauron, P.; Emmenegger, C. *J. Power Sources* **2003**, *118*, 1.
(2) Orimo, S.; Nakamori, Y.; Eliseo, J. R.; Züttel, A.; Jensen, C. M. *Chem. Rev.* **2007**, *107*, 4111.
(3) Graetz, J. *Chem. Soc. Rev.* **2009**, *38*, 73.
(4) Vajeeston, P.; Ravindran, P.; Fjellvåg, H. *J. Alloys Compd.* **2007**, *446−447*, 44.
(5) Buchter, F.; Łodziana, Z.; Remhof, A.; Friedrichs, O.; Borgschulte, A.; Mauron, P.; Züttel, A.; Sheptyakov, D.; Barkhordarian, G.; Bormann, R.; Chłopek, K.; Fichtner, M.; Sørby, M.; Riktor, M.; Hauback, B.; Orimo, S. *J. Phys. Chem. B* **2008**, *112*, 8042.
(6) Černý, R.; Filinchuk, Y.; Hagemann, H.; Yvon, K. *Angew. Chem., Int. Ed.* **2007**, *46*, 5765.
(7) Her, J.-H.; Stephens, P. W.; Gao, Y.; Soloveichik, G. L.; Rijssenbeek, J.; Andrus, M.; Zhao, J.-C. *Acta Crystallogr., Sect. B* **2007**, *63*, 561.
(8) Nickels, E. A.; Jones, M. O.; David, W. I. F.; Johnson, S. R.; Lowton, R. L.; Sommariva, M.; Edwards, P. P. *Angew. Chem., Int. Ed.* **2008**, *47*, 2817.
(9) Filinchuk, Y.; Chernyshov, D.; Dmitriev, V. *Z. Kristallogr.* **2008**, *223*, 649.
(10) Filinchuk, Y.; Rönnebro, E.; Chandra, D. *Acta Mater.* **2009**, *57*, 732.
(11) Frommen, C.; Aliouane, N.; Deledda, S.; Fonneløp, J. E.; Grove, H.; Lieutenant, K.; Llamas-Jansa, I.; Sartori, S.; Sørby, M. H.; Hauback, B. C. *J. Alloys Compd.* **2010**, *496*, 710.
(12) Sato, T.; Miwa, K.; Nakamori, Y.; Ohoyama, K.; Li, H.-W.; Noritake, T.; Aoki, M.; Towata, S.; Orimo, S. *Phys. Rev. B* **2008**, *77*, 104114.
(13) Ravnsbæk, D. B.; Filinchuk, Y.; Černý, R.; Jensen, T. R. *Z. Kristallogr.* **2010**, *225*, 557.
(14) Kim, J.-H.; Jin, S.-A.; Shim, J.-H.; Cho, Y. W. *J. Alloys Compd.* **2008**, *461*, L20.
(15) Aoki, M.; Miwa, K.; Noritake, T.; Ohba, N.; Matsumoto, M.; Li, H.-W.; Nakamori, Y.; Towata, S.; Orimo, S. *Appl. Phys. A* **2008**, *92*, 601.
(16) Kim, Y.; Reed, D.; Lee, Y.-S.; Lee, J. Y.; Shim, J.-H.; Book, D.; Cho, Y. W. *J. Phys. Chem. C* **2009**, *113*, 5865.
(17) Riktor, M. D.; Sørby, M. H.; Chłopek, K.; Fichtner, M.; Hauback, B. C. *J. Mater. Chem.* **2009**, *19*, 2754.
(18) Stavila, V.; Her, J.-H.; Zhou, W.; Hwang, S.-J.; Kim, C.; Ottley, L. A. M.; Udovic, T. J. *J. Solid State Chem.* **2010**, *183*, 1133.
(19) Frankcombe, T. J. *J. Phys. Chem. C* **2010**, *114*, 9503.
(20) Zhang, Y.; Majzoub, E.; Ozolins, V.; Wolverton, C. *Phys. Rev. B* **2010**, *82*, 174107.
(21) Lee, J. Y.; Ravnsbæk, D.; Lee, Y.-S.; Kim, Y.; Cerenius, Y.; Shim, J. H.; Jensen, T. R.; Hur, N. H.; Cho, Y. W. *J. Phys. Chem. C* **2009**, *113*, 15080.
(22) Hagemann, H.; D'Anna, V.; Rapin, J.-P.; Černý, R.; Filinchuk, Y.; Kim, K. C.; Sholl, D. S.; Parker, S. F. *J. Alloys Compd.* **2011**, DOI: 10.1016/j.jallcom.2010.10.068.
(23) Lee, J. Y.; Lee, Y.-S.; Suh, J.-Y.; Shim, J.-H.; Cho, Y. W. *J. Alloys Compd.* **2010**, *506*, 721.
(24) Yoon, S. B.; Kim, J. Y.; Kooli, F.; Lee, C. W.; Yu, J.-S. *Chem. Commun.* **2003**, 1740.
(25) Kang, S.; Chae, Y. B.; Yu, J.-S. *J. Nanosci. Nanotechnol.* **2009**, *9*, 527.
(26) Hammersley, A. P.; Svensson, S. O.; Hanfland, M.; Fitch, A. N.; Häusermann, D. *High Pressure Res.* **1996**, *14*, 235.
(27) Favre-Nicolin, V.; Černý, R. *J. Appl. Crystallogr.* **2002**, *35*, 734.
(28) Rodríguez-Carvajal, J. *Physica B* **1993**, *192*, 55.
(29) Filinchuk, Y.; Chernyshov, D.; Černý, R. *J. Phys. Chem. C* **2008**, *112*, 10579.
(30) Hohenberg, P.; Kohn, W. *Phys. Rev.* **1964**, *136*, B864.
(31) Kohn, W.; Sham, L. J. *Phys. Rev.* **1965**, *140*, A1133.
(32) Kresse, G.; Furthmüller, J. *Phys. Rev. B* **1996**, *54*, 11169.
(33) Kresse, G.; Furthmüller, J. *Comput. Mater. Sci.* **1996**, *6*, 15.
(34) Perdew, J. P.; Burke, K.; Ernzerhof, M. *Phys. Rev. Lett.* **1996**, *77*, 3865.
(35) Blöchl, P. E. *Phys. Rev. B* **1994**, *50*, 17953.
(36) Gross, A. F.; Vajo, J. J.; Van Atta, S. L.; Olson, G. L. *J. Phys. Chem. C* **2008**, *112*, 5651.
(37) Liu, X.; Peaslee, D.; Jost, C. Z.; Majzoub, E. H. *J. Phys. Chem. C* **2010**, *114*, 14036.
(38) Kim, T.-W.; Park, I.-S.; Ryoo, R. *Angew. Chem., Int. Ed.* **2003**, *42*, 4375.
(39) Yoon, S. B.; Chai, G. S.; Kang, S. K.; Yu, J.-S.; Gierszal, K. P.; Jaroniec, M. *J. Am. Chem. Soc.* **2005**, *127*, 4188.
(40) Riktor, M. D.; Sørby, M. H.; Chłopek, K.; Fichtner, M.; Buchter, F.; Züttel, A.; Hauback, B. C. *J. Mater. Chem.* **2007**, *17*, 4939.
(41) Riktor, M. D.; Filinchuk, Y.; Vajeeston, P.; Bardají, E. G.; Fichtner, M.; Fjellvåg, H.; Sørby, M. H.; Hauback, B. C. *J. Mater. Chem.* **2011**, DOI: 10.1039/C1JM00074H.
(42) Fang, Z.-Z.; Kang, X.-D.; Luo, J.-H.; Wang, P.; Li, H.-W.; Orimo, S. *J. Phys. Chem. C* **2010**, *114*, 22736.
(43) Bonatto Minella, C.; Garroni, S.; Pistidda, C.; Gosalawit-Utke, R.; Barkhordarian, G.; Rongeat, C.; Lindemann, I.; Gutfleisch, O.; Jensen, T. R.; Cerenius, Y.; Christensen, J.; Baró, M. D.; Bormann, R.; Klassen, T.; Dornheim, M. *J. Phys. Chem. C* **2011**, *115*, 2497.
(44) Wu, L.; Wang, C.; Chen, X. L.; Li, X. Z.; Xu, Y. P.; Cao, Y. G. *J. Solid State Chem.* **2004**, *177*, 1847.

(45) Wu, L.; Chen, X. L.; Li, H.; He, M.; Dai, L.; Li, X. Z.; Xu, Y. P. *J. Solid State Chem.* **2004**, *177*, 1111.
(46) Stewner, F. *Acta Crystallogr., Sect. B* **1971**, *27*, 904.
(47) Vegas, A.; Cano, F. H.; Garcia-Blanco, S. *Acta Crystallogr., Sect. B* **1975**, *31*, 1416.
(48) Amendola, S. C.; Onnerud, P.; Kelly, M. T.; Petillo, P. J.; Sharp-Goldman, S. L.; Binder, M. *J. Power Sources* **1999**, *84*, 130.
(49) Miwa, K.; Ohba, N.; Towata, S.; Nakamori, Y.; Orimo, S. *Phys. Rev. B* **2004**, *69*, 245120.
(50) Lee, Y.-S.; Kim, Y.; Cho, Y. W.; Shapiro, D.; Wolverton, C.; Ozolins, V. *Phys. Rev. B* **2009**, *79*, 104107.
(51) Soulié, J.-P.; Renaudin, G.; Černý, R.; Yvon, K. *J. Alloys Compd.* **2002**, *346*, 200.